Supplemental Information

This supplemental information contains technical information about the analyses presented in the main paper.

Participant MRI

Approximately half of the participants had a structural MRI. The MRI data were collected on a Siemens Medical Systems 3T Trio with an overall duration of about 15 min. A 3D T1-weighted "MPRAGE" RF-spoiled rapid flash scan in the sagittal plane and a T2/PD-weighted multi-slice axial 2D dual Fast Turbo spin-echo scan in the axial plane were used. The scans had 1 mm^3 resolution and sufficient FoV to cover from the top of the head down to the neck. External head measurements were done on each participant who had a MRI. The measures include semi-circumferences (front and rear sides-circumference from LMA to RMA, top circumferences from Nz to Iz, and from LMA to RMA) and lateral diameters (Nz to Iz, LMA to RMA).

Close Size Head MRI

About half of the infants did not have a structural MRI. For these participants, external head measurements were made during the experimental testing session (see last section). For each participant in the study without a MRI, we calculated the RMS-difference between the six measurements for the participant and any infant within 30 days of the same age with a MRI in the Neurodevelopmental MRI database (Richards, Sanchez, Phillips-Meek, & Xie, 2015; Richards & Xie, 2015). The infant from the database with the closest head measurements was chosen to represent the head model for the participant in the ERP study. In a previous study we found that this “closest MRI” is a good representation of the CDR distribution for an infants “self MRI” (McCleery & Richards, 2012a, b). The close MRI and the infant’s own MRI fit equally well or better than the age-appropriate average MRI used by other infant research (Hämäläinen, Ortiz-Mantilla, & Benasich, 2011; Ortiz-Mantilla, Hämäläinen, & Benasich, 2012; Reynolds & Richards, 2009). We have also tested the fit of a "close MRI" CDR distribution to the "self MRI" in a study in preparation and confirm the use of the close MRI for the CDR analysis.

Electrode Locations on MRI

The MRIcron program (Rorden, http://www.mccauslandcenter.sc.edu/mricro/mricron/) was used to display MRIs and do editing work. A set of fiducials were located on each MRI, including the anterior commissure, posterior commissure and a set of external head locations used for the 10-10 system (e.g., Nz, Iz, LMA, RMA, LPA, RPA, Vz). Details of these procedures are presented in Richards, Boswell, Stevens, & Vendemia, 2015b.

Adult average electrode placement locations were constructed on the young adult (20-24 years) average MRI template from the Neurodevelopmental MRI database (Richards et al., 2015a; Richards & Xie, 2015). The average electrodes were constructed from individual participants who had the positions of the EGI GSN 128 channel electrode net, and HGSN 128 channel electrode net, determined on the head. The electrode positions on the individuals were transformed to the average MRI template and averaged, and fitted to the average MRI template (Richards et al., 2015b).

Age-appropriate average electrode positions were created for average MRI templates of infant templates (3, 4.5, 6, 7.5, 9, and 12 months) from our MRI database (Richards & Xie, 2015). The individual MRIs for each infant making up the age-appropriate average MRI from the Neurodevelopmental MRI database (Richards & Xie, 2015) were used to construct average electrodes for the average template. First, the "virtual 10-10" (Richards et al., 2015) were constructed for each individual MRI. Second, these electrode points on the individual heads were registered to the virtual 10-10 electrodes from the adult electrode configuration (Richards et al., 2015) using “coherent point drift” registration (CPD version 2; Myronenoko et al, 2006; Myronenko & Song, 2010). The resulting 12-degree of freedom affine registration matrix was used to transform the adult average GSN/HGSN electrode configuration into the participant space. This transformed electrode configuration was then fitted to the scalp by finding the nearest location to the scalp from the electrode. The resulting electrode locations were referenced to the AC-coordinate system for that participant. Figure 1 shows an infant participant with the electrodes placed on the MRI. Third, the individual participants virtual 10-10 points were registered to 10-10 points of the age-appropriate average template for that individual, and the individual GSN/HGSN locations were transformed into the age-appropriate average template positions. Finally, these transformed positions were used to construct an average template for that age-appropriate average template. Figure 1 also shows the average electrode positions on the average MRI templates for 6.0 months.

A separate step was used to construct the electrode placement map on individuals used in the source analysis. During the course of an EEG/ERP experiment, individual infants had photos taken of the net placements on the front, rear, right, left, and above the head. The photos were used to visually identify the position of electrodes on the participant MRI volume on the front, rear, left and right of the head (e.g., GSN #’s 17, 73, 57, 101, respectively) and the electrode in the Cz location (e.g., average of GSN electrodes 7, 31, 55, 80, 106). These electrodes were visually located on the scalp of the participant’s MRI volume and translated into the AC-PC space of that individual. The electrode placement map was constructed for the individual MRI by registering the electrode positions on the individual MRI (from photo) to the same electrode positions on the average electrode map for the age-appropriate MRI average, and the average electrodes were transformed into the AC-coordinate system for that participant and fitted to the MRI head (Richards et al., 2015b).

Supplemental Information in Richards (2013)

We rely on methods presented in Richards (2013), both the main text and the supplemental information for that study. The following sections include details found either in the Supplemental Information or the main paper for that study.

Virtual 10-20 Electrodes

The GSN 128 and Hydrocel GSN 128 Sensornet channel electrodes were combined into groups of electrodes representing "virtual 10-20" electrodes. We used the same procedure and rationale for transforming groups of EGI electrodes into their 10-10 equivalents. Figure 2 shows the connections between the virtual electrode positions of the Hydrocel GSN128 electrrode net overlaid on the 6-month-old average MRI template (colors), and the 10-10 virtual electrode positions for this MRI template. The virtual electrode combinations were chosen to overlay the associated 10-10 positions. The GSN and HGSN electrode nets have different numbering systems, so we used different numbers for each net type for the translation to virtual 10-10 electrodes. The channel numbers and positions are given in Table 1..

Head Segmentation

The materials in the head were segmented, including scalp, skull, CSF, white matter, gray matter, nasal cavity, and eyes (Richards, 2002, 2005, 2013). The segmentation was mapped into three-dimensional "Finite Element Method" (FEM) wireframes and the conductivity values were assigned to each tetrahedral element proportional to the amount of segmented material in the tetrahedron. Details of this procedure are given in Richards (2013, Supplemental Information). Figure 3 shows a wireframe placed on the MRI of an individual 6-month-old participant.

The gray matter segmentation was used to construct the locations of sources for the current density reconstruction. A three-dimensional wireframe was used that identified individual tetrahedral volumes for the current sources. This was done separately on each MRI. Figure 3 shows a source wireframe placed on the MRI of an individual 6-month-old participant.

Atlases

Three atlases were constructed on the individual participants MRIs. The LONI Probabilistic Brain Atlas (LPBA; Shattuck, et al., 2008) and the Hammers atlas, based on MRIs from the Information Exchange for the Internet (Hammers atlas; Heckemann, Hajnal, Aljabar, Rueckert, & Hammers, 2006; Heckemann, et al., 2003) were constructed on individual participants. Details of the construction of these atlases for individual participants may be found in Phillps et al. (2012) and Fillmore et al. (submitted); and we have used these atlases in previous work to define ROIs for cortical source analysis (Richards, 2013; also see Supplemental Information for Richards, 2013). The LPBA atlas has 56 areas defined for the cortex, sub-cortex, brainstem, and cerebellum. The Hammers atlas has 83 areas defined from the cortex, sub-cortex, brainstem, and cerebellum. The third atlas was an automatically constructed lobar atlas that defined the major lobes (e.g., frontal, temporal) of the cortex, some sub-lobar cortical areas (e.g., fusiform gyrus), subcortical (e.g., striatum, thalamus), cerebellum and brainstem. This atlas was constructed from a manually-labeled age-appropriate lobar atlas transformed into the participant's MRI space, the adult MRI average template lobar atlas transformed into the participant space, and the relevant segments from the LPBA and Hammers atlas. These atlases were combined with a majority vote procedure to define a lobar atlas for each individual MRI.

The atlases were used to define several anatomical areas by identifying common designations from each of the atlases, and ROIs were mapped for each participant MRI. These

ROIs are listed in the main paper, and show in Figure 2 of the main paper. They were chosen based on theoretical grounds or previous research examining face-sensitive brain areas in adult participants, or the Nc-source areas in infants (Reynolds & Richards, 2005; Reynolds et al., 2010). The primary ones of interest were the middle fusiform gyrus, anterior fusiform gyrus, superior temporal gyrus and superior temporal sulcus, lateral inferior occipital lobe, orbital-frontal gyrus, ventral anterior cingulate, dorsal anterior cingulate. Additionally, we used other ROIs that could account for ERP activity that might not be specifically related to face processing. These include the occipital lobe, parietal lobe, middle and inferior temporal gyrus, lingual gyrus, parahippocampal gyrus, frontal pole. Supplemental Information Table 2 has a list of the ROIs, and the labels for the anatomical areas taken from the lobar, Hammers, or LPBA40 atlas.

References

Fillmore, P., Richards, J. E., Phillips-Meek, M. C., Connington, A. & Stevens, M (2014a). *Stereotaxic MRI brain atlases for infants from 3 to 12 months*.

Hamalainen, J. A., Ortiz-Mantilla, S., & Benasich, A. A. (2011). Source localization of event-related potentials to pitch change mapped onto age-appropriate MRIs at 6 months of age. *Neuroimage, 54*(3), 1910-1918. doi: 10.1016/j.neuroimage.2010.10.016

Hammers, A., Allom, R., Koepp, M. J., Free, S. L., Myers, R., Lemieux, L., . . . Duncan, J. S. (2003). Three-dimensional maximum probability atlas of the human brain, with particular reference to the temporal lobe. *Hum Brain Mapp, 19*(4), 224-247. doi: 10.1002/hbm.10123

Heckemann, R. A., Hajnal, J. V., Aljabar, P., Rueckert, D., & Hammers, A. (2006). Automatic anatomical brain MRI segmentation combining label propagation and decision fusion. *Neuroimage, 33*(1), 115-126. doi: 10.1016/j.neuroimage.2006.05.061

Heckemann RA, H. T., Leung K, Hill DLG, Hajnal JV, Rueckert D. (2003). *Information Extraction from Medical Images (IXI): Developing an e-Science Application Based on the Globus Toolkit*. Nottingham, UK.

McCleery, J. P., & Richards, J.E. (April, 2012). *Comparing realistic head models for cortical source locationization of infant event-related potentials.* . Paper presented at the Poster presented at the 3rd UK Paediatric Neuropsychology Symposium, University College London Institute for Child Health, London, England.

McCleery, J. P., & Richards, J.E. (June, 2012). *Comparing realistic head models for cortical source locationization of infant event-related potentials.* . Paper presented at the International Conference on Infant Studies,

, Minneapolis, MN.

Myronenko, A., Song, X., & Carreira-Perpinan, M. (2007). Non-rigid point set registration: Coherent point drift. . *Advances in Neural Information Processing Systems -- Proceedings of the 2006 Conference., 19*, 1009-1016.

Myronenko, A., & Song, X. . (2010). Point Set Registration: Coherent Point Drift. *IEEE Transactions on Pattern Analysis and Machine Intelligence,, 32*, 2262-2275.

Ortiz-Mantilla, S., Hamalainen, J. A., & Benasich, A. A. (2012). Time course of ERP generators to syllables in infants: a source localization study using age-appropriate brain templates. *Neuroimage, 59*(4), 3275-3287. doi: 10.1016/j.neuroimage.2011.11.048

Phillips, M. C., Richards, J. E., Stevens, M. & Connington, A. . (2013). *A stereotaxic MRI brain atlas for infant participants.* Paper presented at the Society for Research in Child Development, Seattle, WA.

Reynolds, G. D., Courage, M. L., & Richards, J. E. (2010). Infant attention and visual preferences: converging evidence from behavior, event-related potentials, and cortical source localization. *Dev Psychol, 46*(4), 886-904. doi: 10.1037/a0019670

Reynolds, G. D., & Richards, J. E. (2005). Familiarization, attention, and recognition memory in infancy: an event-related potential and cortical source localization study. *Dev Psychol, 41*(4), 598-615. doi: 10.1037/0012-1649.41.4.598

Reynolds, G. D., & Richards, J. E. (2009). Cortical source localization of infant cognition. *Dev Neuropsychol, 34*(3), 312-329. doi: 10.1080/87565640902801890

Richards, J. E. (2002). *Using EMSE and EGI for source analysis display and illustration.* Retrieved from http://jerlab.psych.sc.edu/pdf/emseegi.pdf

Richards, J. E. (2006). *Realistic cortical source models of ERP.* Retrieved from http://jerlab.psych.sc.edu/PDF%20Files/RealisticSourceModels.pdf

Richards, J. E. (2013). Cortical sources of ERP in prosaccade and antisaccade eye movements using realistic source models. *Front Syst Neurosci, 7*, 27. doi: 10.3389/fnsys.2013.00027

Richards, J. E., Boswell, C., Stevens, M., & Vendemia, J. M. (2015). Evaluating methods for constructing average high-density electrode positions. *Brain Topogr, 28*(1), 70-86. doi: 10.1007/s10548-014-0400-8

Richards, J. E., Sanchez, C., Phillips-Meek, M., & Xie, W. (2015). A database of age-appropriate average MRI templates. *Neuroimage*. doi: 10.1016/j.neuroimage.2015.04.055

Richards, J. E. X., W. (2015). Brains for all the ages: Structural neurodevelopment in infants and children from a life-span perspective. In J. Bensen (Ed.), *Advances in Child Development and Beahvior* (Vol. 48).

Sanchez, C. E., Richards, J. E., & Almli, C. R. (2011). Neurodevelopmental MRI brain templates for children from 2 weeks to 4 years of age. *Dev Psychobiol, 54*(1), 77-91. doi: 10.1002/dev.20579

Shattuck, D. W., Mirza, M., Adisetiyo, V., Hojatkashani, C., Salamon, G., Narr, K. L., . . . Toga, A. W. (2008). Construction of a 3D probabilistic atlas of human cortical structures. *Neuroimage, 39*(3), 1064-1080. doi: 10.1016/j.neuroimage.2007.09.031

Table 1, Virtual 10-10 electrode clusters. The GSN and HGSN nets have different numbering systems. The electrodes chosen surround the virtual 10-10 electrode on the average MRI template (Figure 2)

Component	**10-10 Virtual Electrode**	**HGSN Electrodes**	**GSN Electrodes**
N290	Parietal Occipital7 (PO7)	59, 65, 66	59, 65, 66
	Parietal Occipital8 (PO8)	84, 90, 91	85, 91, 92
	Parietal Occipital9 (PO9)	64, 65, 68, 69	64, 65, 69, 70
	Parietal Occipital10 (PO10)	89, 90, 94, 95	90, 91, 95, 96
	Parietal7 (P7)	51, 58, 59	51, 58, 59
	Parietal8 (P8)	91, 96, 97	92, 97, 98
	Parietal9 (P9)	57, 58, 63, 64	57, 58, 63, 64
	Parietal10 (P10)	95, 96, 99, 100	96, 97, 100, 101
	Temporal Parietal7 (TP7)	46, 50, 51	47, 50, 51
	Temporal Parietal8 (TP8)	97, 101, 102	98, 102, 103
	Temporal Parietal9 (TP9)	50, 56, 57	50, 56, 57
	Temporal Parietal10 (TP10)	100, 101, 107	101, 102, 108
P400	OccipitalZ (Oz)	71, 75, 76	72, 76, 77
	Occipital1 (O1)	66, 70, 71	66, 71, 72
	Occipital2 (O2)	76, 83, 84	77, 84, 85
	InionZ (Iz)	74 75, 81, 82	75, 76, 82, 83
	Inion1 (I1)	69, 70, 73, 74	70, 71, 74, 75
	Inion2 (I2)	82, 83, 88, 89	83, 84, 89, 90
	Parietal Occipital7 (PO7)	59, 65, 66	59, 65, 66
	Parietal Occipital8 (PO8)	84, 90, 91	85, 91, 92
	Parietal Occipital9 (PO9)	64, 65, 68, 69	64, 65, 69, 70
	Parietal Occipital 10 (PO10)	89, 90, 94, 95	90, 91, 95, 96
Nc	FrontalZ (Fz)	5, 10, 11, 12, 16, 18	5, 10, 11, 12, 16, 19
	Frontal CentralZ (FCz)	5, 6, 7, 12, 106	5, 6, 7, 12, 107
	CentralZ (Cz)	7, 31, 55, 80, 106	7, 32, 55, 81 1037

Table 2. Regions-of-interest (ROIs) and anatomical regions with labels from the lobar, Hammers, and LPBA40 atlases. The left column are lateralized, and are presented from posterior-anterior and lateral-medial. The right column are bilateral and presented from posterior to anterior.

Lateral inferior occipital lobe	
LPBA	
65	L inferior occipital gyrus, lateral part
66	R inferior occipital gyrus, lateral part
Inferior and middle temporal gyrus	
LPBA	
83	L middle temporal gyrus
84	R middle temporal gyrus
85	L inferior temporal gyrus
86	R inferior temporal gyrus
Medial inferior occipital lobe	
LPBA	
65	L inferior occipital gyrus, medial part
66	R inferior occipital gyrus, medial part
Middle fusiform gyrus	
Lobar	Fusiform gyrus, middle part
Hammers:	
15	Lateral occipitotemporal gyrus right, middle part
16	Lateral occipitotemporal gyrus left, middle part
LPBA	
91	L fusiform gyrus, middle part
92	R fusiform gyrus, middle part
Anterior fusiform gyrus	
Lobar	Fusiform gyrus, anterior part
Hammers:	
15	Lateral occipitotemporal gyrus right, anterior part
16	Lateral occipitotemporal gyrus left, anterior part
LPBA:	
91	L fusiform gyrus, anterior part
92	R fusiform gyrus, anterior part
Lingual gyrus	
Hammers	
64	Lingual gyrus left
65	Lingual gyrus right
LPBA	
89	L lingual gyrus
90	R lingual gyrus
Parahippocampal gyrus	
Hammers	
9	Parahippocampal and ambient gyri right
10	Parahippocampal and ambient gyri left
LPBA	
87	L parahippocampal gyrus
88	R parahippocampal gyrus

Occipital lobe	
Lobar	Occipital pole
Hammers	
66, 67	Cuneus (left, right)
LPBA	
67 68	L, R Cuneus
Middle occipital lobe	
LPBA	
63, 64	L, R middle occipital gyrus
Superior occipital lobe	
LPBA	
61 62	L, R superior occipital gyrus
Superior parietal lobe	
Hammers	
62, 63	Superior parietal gyrus left, right
LBPA	
43, 44	L, R_superior_parietal_gyrus
Posterior cingulate gyrus	
Hammers	
26, 27	Cingulate gyrus left, right, posterior part
LPBA	
121, 122	L, R_cingulate_gyrus, posterior part
Dorsal-anterior cingulate gyrus	
Hammers	
24, 25	Cingulate gyrus, anterior (supragenual), left, right, superior to anterior commissure
LPBA	
121, 122	L R cingulate_gyrus, anterior part, superior to AC
Ventral-anterior cingulate	
Hammers	
76. 77	Subgenual anterior cingulate gyrus (right, left)
78, 79	Subcallosal area (right, left)
80, 81	Pre-subgenual anterior cingulate (right, left)
24, 25	Cingulate gyrus, anterior (supragenual) (right, left), inferior to anterior commissure
LPBA	
121, 122	L R cingulate_gyrus, anterior part, inferior to AC
Orbito-frontal gyrus	
Hammers	
52, 53	` straight gyrus (right and left),
68, 69	, medial orbital gyrus (right and left),
LPBA	
29,30	L, R middle orbitofrontal gyrus
33,34	L, R , gyrus rectus

Superior temporal gyrus		Frontal pole	
LPBA		Lobar	Frontal pole
81	L superior temporal gyrus		
82	R superior temporal gyrus		
Temporal pole			
Hammers			
5	Anterior temporal lobe, medial part right		
6	Anterior temporal lobe, medial part left		
7	Anterior temporal lobe, lateral part right		
8	Anterior temporal lobe, lateral part left		
82	Superior temporal gyrus, anterior part left		
83	Superior temporal gyrus, anterior part left		
Superior temporal sulcus			
LBPA			
81 & 83	Intersection (2 mm ea) of L superior temporal gyrus and L middle temporal gyrus		
82 & 84	Intersection (2 mm ea) of R superior temporal gyrus and R middle temporal gyrus		

Figure 1. Electrode placement for a six-month old infant, and the 6-month-old average MRI template

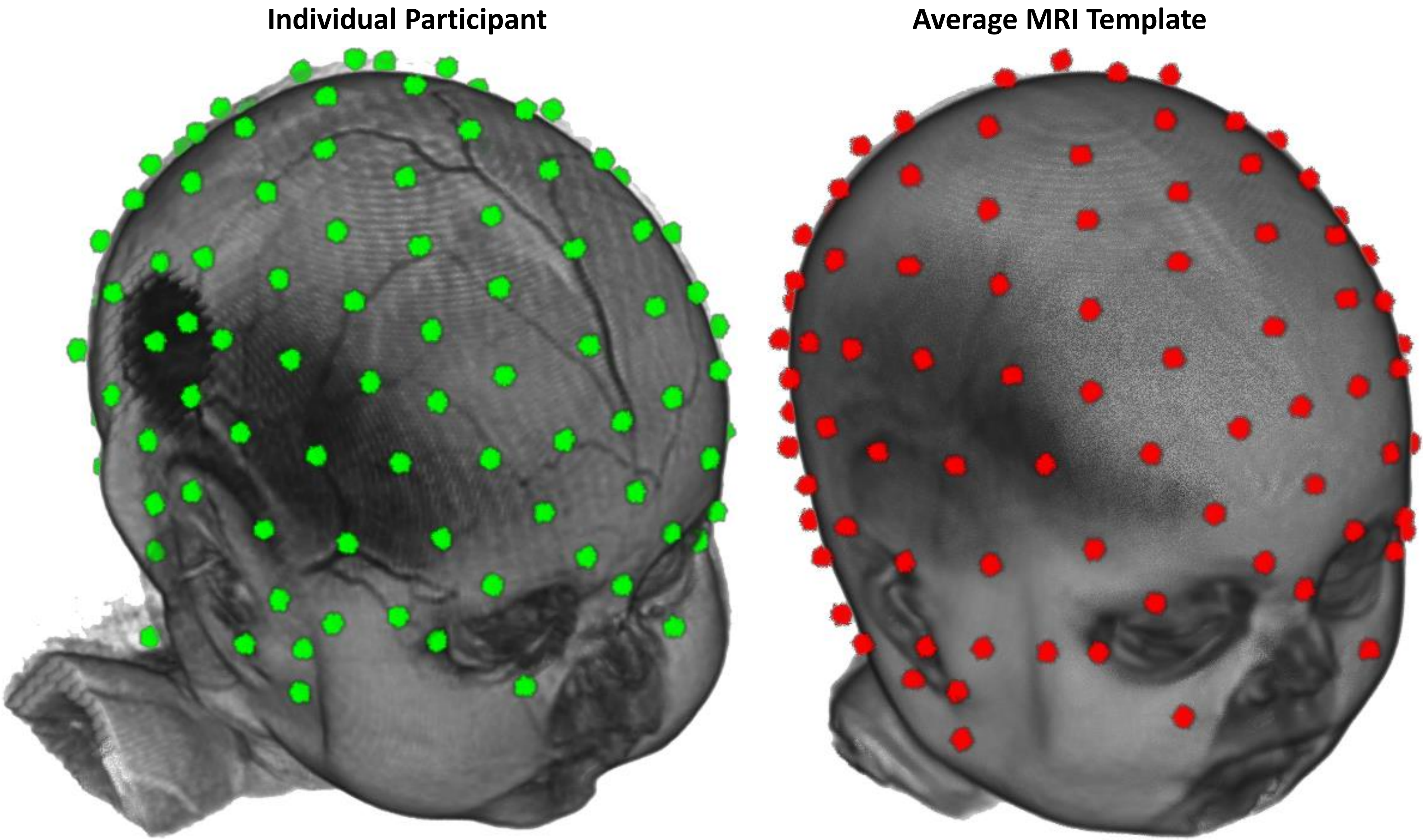

Figure 2. ***Hydrocel GSN128 electrode connections for inferior-posterior virtual electrodes, and actual 10-10 locations. This is plotted on the age-appropriate 6-0 months average MRI template***

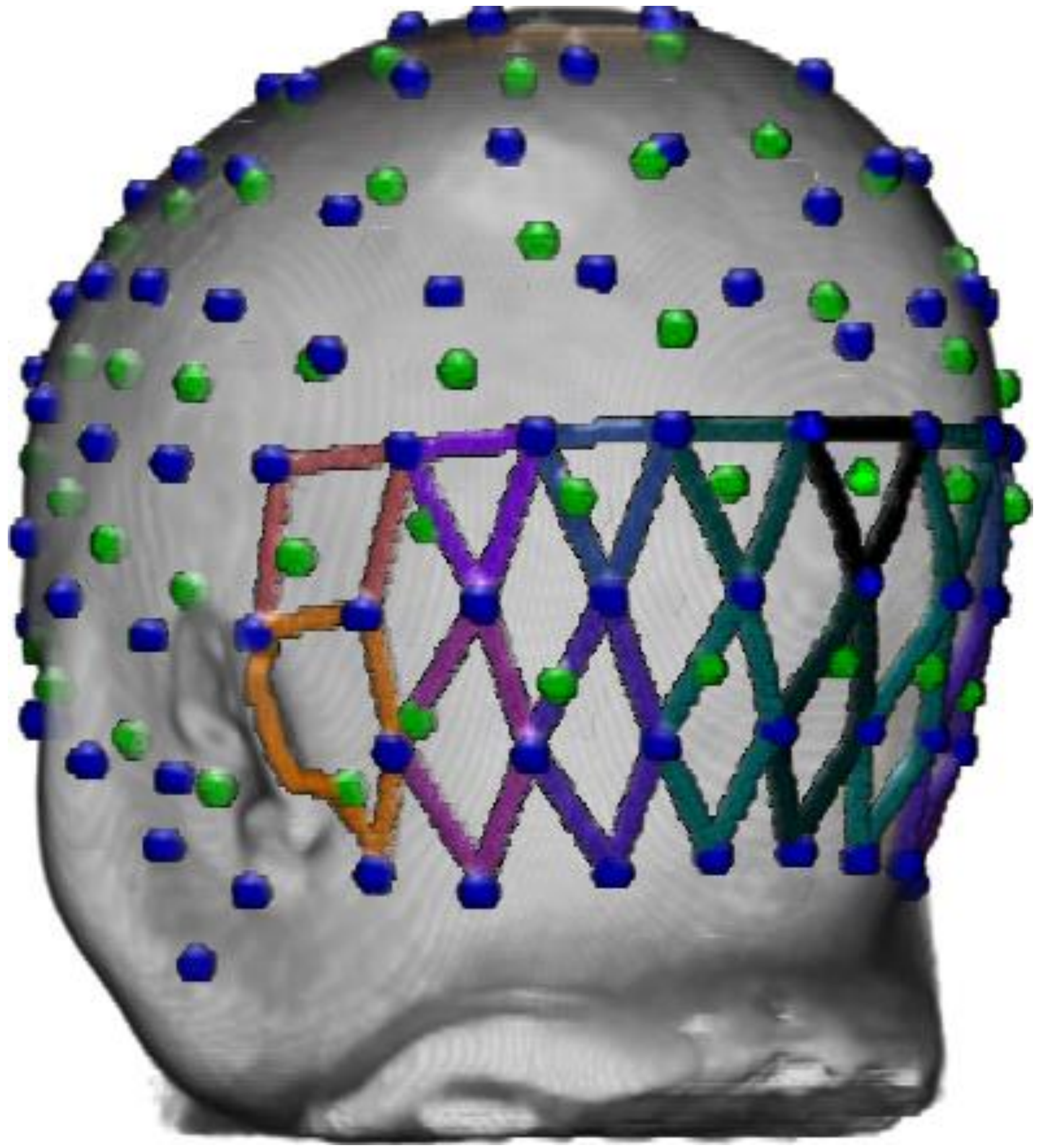

Figure 3. *FEM model and source volume in an individual infant MRI*